J. Water Environ. Nanotechnol., 8(3): 229-240 Summer 2023

ORIGINAL RESEARCH PAPER

Hibiscus Rosasinesis Flower Extract Mediated Ni/ZnO nanoparticles for Visible Light Driven Photocatalytic Degradation of Roseaniline Dye as a Pollutant

Rajendaran Karthiga[1], Saravanan Karthikarani [2,*]

[1] PG and Research Department of Chemistry, Cardamom Planters' Association College, Bodinayakanur, Theni, Tamilnadu, India
[2] Department of Physics, Cardamom Planters' Association College,Bodinayakanur,Theni, Tamilnadu, India

Received: 2023-03-04 Accepted: 2023-06-06 Published: 2023-08-09

ABSTRACT
The green fabricated photocatalyst is promising material and could be applied for waste-water remediation and other ecological applications. Hibiscus floral extract surface modified Ni-doped ZnO (HFNZO) was obtained by simple co-precipitation. The flowers have secondary metabolites such as phenolic compounds named flavonoids; tannins are turned to be reluctant to synthesize Ni/ZnO nanoparticles from the precursor. The prepared nanoparticles were examined by various characterization for their optical, structural, and surface morphology properties were determined using Uv-Drs, FTIR, XRD, SEM, TEM, EDX, and XPS techniques. Absorption spectral shift of visible light region (redshift) and band gap reduction for ZnO (ZO), hibiscus modified ZnO (HFZO), and hibiscus surface modified Ni-doped ZnO (HFNZO) properties were studied, and shows a reduction in the band gap of the nanoparticles from 3.0eV – 1.65 eV. Results obtained from XRD analysis show that the synthesized HFNZO nanoparticles have a particle size of about 24.85 nm which is also confirmed by TEM analysis. A 98% visible-light-mediated degradation of the aqueous Rose aniline hydrochloride (RA) of 20 µM solution containing HFNZO of 0.05 g/L nanoparticles has been achieved within 90 min. It follows pseudo first order Kinetic and the mechanism of generation of hydroxyl group due to flower extract surface modification and doping has been explained.

Keywords: Hibiscus rosasinesis, Doping, HFNZO, Photocatalysis, Rose aniline.

How to cite this article
Karthiga R., Karthikarani S., Hibiscus Rosasinesis Flower Extract Mediated Ni/ZnO nanoparticles for Visible Light Driven Photocatalytic Degradation of Roseaniline Dye as a Pollutant. J. Water Environ. Nanotechnol., 2023; 8(3): 229-240.
DOI: 10.22090/jwent.2023.03.003

INTRODUCTION

It is necessary to remove dye contaminants from the effluents before discharged into the environment, not only for aesthetic reasons but Environmental problems associated with harmful organic dyes pollutants in water are the driving forces for sustained fundamental and applied research in the area of environmental remediation[1],[2] Dye adversely impacts on biological oxygen demand (BOD) and chemical oxygen demand (COD). Textile dyes and their metabolites act as mutagenic, toxic, and carcinogenic agents. They appear to cross the food chains, leading to biomagnification, so that species have a higher level of contamination at a higher trophic level relative to their prey [3].In recent years, there has been a lot of interest in the heterogeneous photocatalytic destruction of refractory organic water contaminants by semiconductors [4], [5], [6]. Wide-bandgap semiconductor photocatalysts like ZnO and TiO_2 have been shown in earlier research to destroy a variety of organic contaminants when exposed to UV light, which opens up the possibility of eliminating harmful compounds [7], [8]. considerable attempts have been focused

* Corresponding Authors Email: *skarthika1121@gmail.com*

on developing photocatalysts that are active in the most abundant part of the solar spectrum, visible light (λ≥420 nm)[9][10]– [12]. This has inspired many researchers to learn more about ZnO's characteristics in various photocatalytic processes.

Several methods have been reported in the review for the preparation of undoped and doped ZnO nanoparticles like sol-gel[13], solution combustion[14], spray atomization[15], controlled synthesis[16], and hydrothermal [17] Alternatives to these methods for producing ZnO nanoparticles in an environmentally acceptable way include plant extract or plant biomass.

- ZnO/NiO nanocomposite from Clitoriaternatea flower extract [18],
- $ZnFe_2O_4$@ZnO nanocomposites using *Chrysanthemum* spp. floral waste for photocatalytic dye degradation [19],
- CuO–ZnO–C nanocomposites using marigold [20],
- green synthesis of ZnO nanoparticles by plant biomass [21]
- flower-like ZnO structures using Arabic and Karaya Gums [22].

Hibiscus rosasinesis flowers have been demonstrated to have protective effects against the tumor, cancer development, anti-implantation, and anti-spermatogenic properties[23], [24]. It has been found that the leaves and petals encourage hair development and help an ulcer heal[25]. According to a phytochemical investigation, the aqueous extract of Hibiscus rosasinesis flowers contains tannins, saponins, alkaloids, steroids, and flavonoids. These phytochemicals present in the Hibiscus rosasinesis flowers can function as a capping and reducing agent.

However, due to the rapid recombination rate of the photogenerated electron/hole pairs in this technique, the photocatalyst needs to be substantially enhanced before it can be commercialized. Therefore, to increase photocatalytic effectiveness, it is imperative to inhibit the recombination of photogenerated electron-hole pairs in semiconductors [26]. Doping of Nickel which is a good conductor of heat and electricity and loses its metallic character very slowly. The ionic radii of Ni^{2+} (0.69 Å) and Zn^{2+} (0.74 Å) are very close and they have the same valance with the same structure[27] which can be easily replaced by Zn^{2+} in ZnO lattice without changing the hexagonal structure of ZnO.

Based on the aforesaid facts and due to the simplicity, easy approach, versatility, and cost-effectiveness, the co-precipitation method was used for the preparation of Ni/ZnO with the addition of flower extract of Hibiscus rosasinesis which act as a capping agent in the current study. The synthesized nanoparticles were investigated on the structural, optical and photocatalytic properties basis. The photocatalytic activity ofZO, HFZO and HFNZOwas appraised for RA dye under Visible light irradiation.However, it would be interesting to study the time dependent photocatalytic response of HFNZO for the degradation of the RA for the first-time adsorption desorption isotherm has achieved within 15 min using flower extract as a surface modifier.

EXPERIMENTAL

Materials and Method

The entire chemicals were purchased from Merck, India of analytical grade and Fresh flower of Hibiscus rosasinesis were collected from the Theni District. To eliminate salts and other associated pollutants, the freshly harvested Hibiscus rosasinesis flowers were washed and they were then chopped into small pieces. 10 g of flower with 100 ml of double-distilled water are heated at 100°C for 30 minutes. The heated filtrate was filtered through Whatman No. 1 and used for subsequent research which is stored in a refrigerator at 4°C [28], [29].

Using a magnetic stirrer, 5.5 g of zinc acetate dehydrate was dissolved in 50 mL of distilled water, and to the above mixture 5 mL of floral extract was added dropwise. The pH of the solution was then raised to 12 with 0.1 N NaOH for the formation of the precipitate. 0.02 molar solution of $NiCl_4$ was added to the aforementioned precipitate. The resulting suspension was agitated for two hours. The precipitate of flower extract modified Ni/ZnO (HFNZO) had been washed with distilled water and allowed to air dry. The HFNZO nanoparticle was kept in a hot air oven for an hour. The same process is carried out without the use of $NiCl_4$ for the preparation of flower extract-modified ZnO. For comparison, undoped ZnO was prepared in the same way without the addition of Ni and flower extract. Finally, the samples were coded by ZO, HFZO, and HFNZO for ZnO, Flower extract-modified ZnO, and flower extract-modified Ni-doped ZnO respectively.

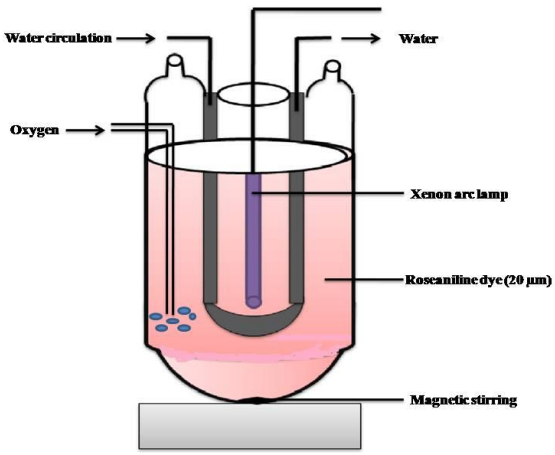

Fig. 1 Schematic diagram of photoreactor for RA degradation

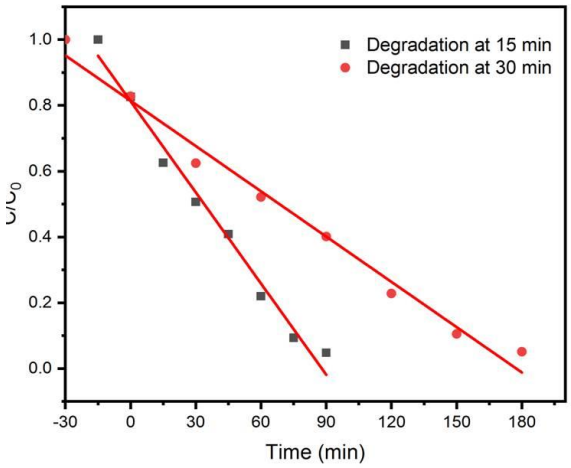

Fig. 2. Adsorption isotherm for 15 and 30 min of degradation of RA

Characterization

UV-VIS light spectra of the synthesized nanoparticles were recorded (l25 spectrophotometer, Perkin Elmer Germany). The same amount of different samples was considered for UV-VIS data analysis. Powder X-ray diffraction (Miniflex 600, Rigaku, Sustin, TX, USA) patterns of the synthesized materials were analyzed in the range of 2q from 20° to 80° using powder diffractometer, Model D8, BRUKER AXS, by Cu Ka radiation (a ¼ 0.15425 nm). The FT-IR studies of the prepared QFW adsorbent were characterized using a JASCO spectrophotometer (JASCO-FT-IR-460 plus) with KBr pelletization in a wide range wavelength ranging from 400 cm^{-1} and 4000 cm^{-1}. A scanning electron microscope (JEOL, JSM - 6380 A, Tokyo, Japan) was used to image the nanoparticles in both secondary and backscattered electron modes. The elemental analysis was detected by energy-dispersive X-ray spectroscopy (Jeol, JSM - 6380 A, Tokyo, Japan). The particle shape was determined by transmission electron microscopy (TEM, Tecnai G20, FEI, Eindhoven, The Netherlands). XPS analysis was done using a VG Micro tech Multi lab ESCA 2000 equipment with a CLAM MCD detector, Al Kα (hν = 1453.6 eV) radiation, and using 50 and 20 eV pass energy for the acquisition of the survey and high-resolution spectra, respectively. A pH meter from EUTECH was used to track pH.

Procedure for evaluation of photocatalytic activity

Roseaniline Hydrochloride (RA) is a cationic dye that was used as a model pollutant and used for photocatalytic studies for synthesized HFNZO [30]. The schematic diagram of the photoreactor was shown in Fig. 1 in which a cylindrical glass vessel, 300 mL of RA solution with a starting concentration of 20 µM was added. An inner jacket of water circulating was placed around it to keep the lamp cool. An air pump was used to continually bubble air into the aliquot, providing a steady source of dissolved oxygen from the bottom of the reactor. Because, the oxygen combines with produced hydroxyl radicals (˚OH) along with other oxidants, e.g., superoxide radical anion ($O_2^{-\circ}$), can further mineralize organic compounds to end products (water and CO_2)[31][32]. Then the vessel was filled with the photocatalyst. Before being exposed to irradiation, the aqueous suspension was stirred continuously for 15 minutes in the dark to achieve adsorption isotherm and it is compared with 30 minutes as shown in Fig. 2. Both kinetic plots show the same R^2 value of 0.9862 and 0.9847 for 15 and 30 min respectively which confirms that the adsorption isotherm has been achieved within 15 min. 300W Xenon arc lamps with a UV-cut-off filter were used as a visible light source. 5 mL of aliquot samples were withdrawn from the reaction mixture at a regular time interval of 15 min. The sampled suspensions were then centrifuged at 4000 rpm for 20min to remove the catalyst and the residual dye concentration was analyzed by UV–vis spectrophotometer.

$$\text{Degradation efficiency (\%)} = \frac{C_0 - C}{C_0} \times 100 \quad (1)$$

Where C_0(µM) is the initial concentration of RA and C (µM) is the concentration of RA after a certain irradiation time.

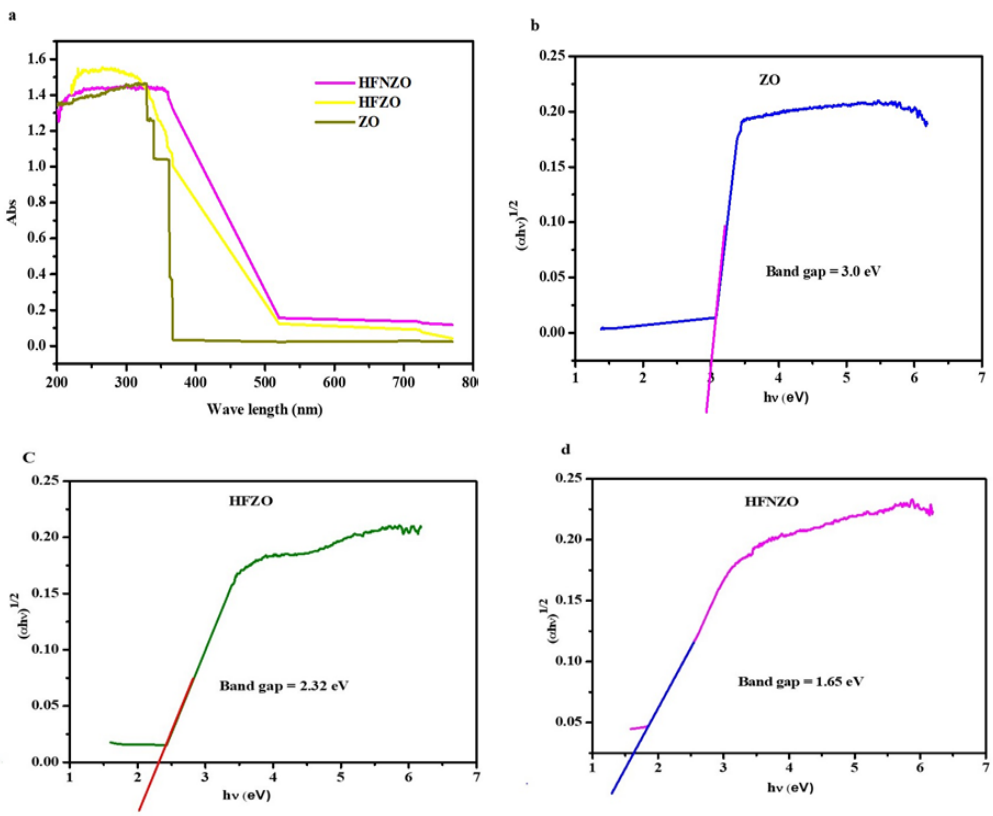

Fig. 3. (a)UV-Visible diffuse reflectance spectroscopy of ZO, HFZO, and HFNZO (b-d)Tauc plot of ZO, HFZO, and HFNZO

RESULT AND DISCUSSION

Characterization

UV-Visible diffuse reflectance spectroscopy was measured at room temperature between 200-800 nm range of wavelength as shown in Fig. 3. (a). The band gap depends on various factors, including grain size, oxygen deficiency, surface roughness, and lattice strain[33] The smaller band gap will easily categorize a photocatalytic reaction of the nanoparticles and show good photocatalytic activity for the degradation of RA. Due to the smaller band gap, the electron is easily excited from the valence band to the conduction band. Subsequent findings indicate that doping of Ni and floral extract modification decreases the band gap [34]. This can be attributed to the smaller particle size and greater surface roughness.

$$\alpha = \frac{C(h\nu - E_g^{bulk})^2}{h\nu} \quad (2)$$

The above equation [35] extrapolates the linear section of the α^2 versus hvgraphs to yield the optical band gap E_g of the nanoparticles.Fig. 3(b), 1(c), and 1(d) show the tauc plot of ZO, HFZO, and HFNZO, respectively. ZO, HFZO, and HFNZO were reported to have 3.0 eV, 2.32 eV, and 1.65 eV, respectively of their band gap which is red-shifted [36]. HFNZO results in a decreased band gap which has greater visible light photocatalytic activity than ZO and HFZO.

In Fig. 4. two prominent absorption peaks at 437 cm^{-1} and 505 cm^{-1}, which correspond to the hexagonal primitive lattice of ZnO and are in good agreement with the XRD conclusion [37], were seen for all of the samples. The bonding between Zn and O is reflected by the peaks at 611 cm^{-1}. Ni-O stretching vibration is thought to be responsible for the peak at 735 cm^{-1}[38]. The peak at 1369 cm^{-1} and 1507 cm^{-1} was caused by the rocking of C-H and C=Cstretching, and the peaks at 2349 cm^{-1} are ascribed to the stretching vibration of CO_2[39]. Variations from 1055 cm^{-1} and 619 cm^{-1} to 1125 cm^{-1} and 635 cm^{-1} imply that proteins, amines, and polyphenols functional group in the flower extract. ZnO nanoparticles may interact with phytochemicals in the flower extract, building a capping over the ZnO[40].

The phase structure of synthesized ZO, HFZO,

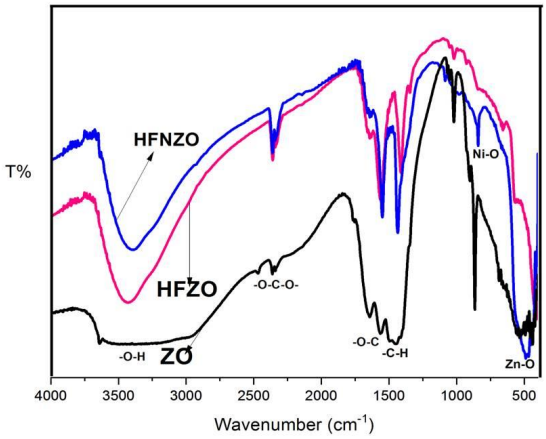

Fig. 4. FT-IR spectrum of ZO, HFZO and HFNZO

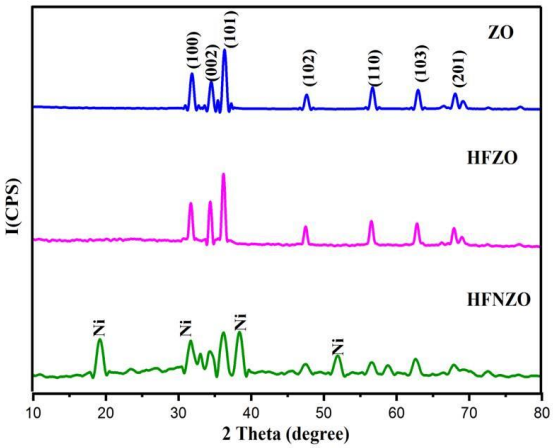

Fig. 5. ZO, HFZO and HFNZO pattern of XRD

and HFNZO nanoparticles was portrayed by XRD pattern and displayed in Fig. 5. According to JCPDS no. 65-3411, The diffraction edges of ZnO acquired at 31.82˚, 34.47˚, 36.30˚, 47.58˚, and 56.64˚ that can be indexed to reflections from the (100), (002), (101), (102), and (110) planes of hexagonal ZnO, respectively. In addition to hexagonal ZnO peaks, the HFNZO nanoparticles XRD pattern also revealed peaks from the (111), (200), (220), and (311) planes corresponding to Ni (JCPDS no 89-7129). Debye's Scherrer equation [27] has been used to estimate the average crystallite size:

$$D = \frac{K\lambda}{\beta \cos\theta} \tag{3}$$

where K is the shape factor, and β is the most intense 2θ peak whole width at half height maximum (0.89). The incident angle and wavelength of X-rays are represented by θ and λ, respectively. ZO, HFZO, and HFNZO nanoparticles' average particle sizes were determined to be 35.12 nm, 31.58 nm, and 24.85 nm, respectively[36], [38]

The morphological structure of ZO, HFZO, and HFNZO were studied by SEM. The results are displayed in Fig. 4. The irregular plate with aggregation is seen in Fig. 6(a) with nanoparticles having almost spherical shapes [5]. Such aggregation and flaky agglomeration could be due to a high surface energy of the nanoparticles and also perhaps due to densification of the narrow space between nanoparticles. In Fig. 6 (b) it seems that the aggregation, as well as the flake thicknesses, becomes less for ZnOnanoparticlesand after additional flower extract Hibiscus rosasinesis. On doping with Ni, the SEM is revealed to be needle-shaped. It has become clear that the metal and added floral extract has a significant effect on the nanoparticle's shape. The new morphology of zinc oxide nanoparticles made them suitable for photodegradation. The EDX spectra obtained at various sites are depicted in Fig. 6(a, b, and c). They only contain the predicted elements (Zn, Ni, and O) with no other contaminant elements. For HFNZO, the typical atomic percentage ratio of Zn, Ni, and O is around 6.95:2.39:80:60.

To further elucidate the size and structures of nanoparticles and nanoneedles TEM was carried out. Fig. 7 shows the TEM image of HFNZO indicates the TEM image of doped and flower extract-modified ZnO nanoparticles of sizes varying from 22 to 28 nm. The varying size is due to the agglomeration of particles. The difference in the crystal growth velocities in different directions causes changes in surface morphology. The addition of Ni ions in the precursor solution induces a thermodynamic barrier. It has been observed that doping plays an important role in producing nanoneedles which is corroboration with the earlier reports[41].

Fig. 8 shows the XPS results for the chemical compositions and valence states properties of the HFNZO nanoparticles. Two sharp peaks are observed corresponding to the spin-orbit of Zn 2p3/2 and Zn 2p1/2 at binding energies 1021.1 eV and 1044.4 eV respectively. The broad peak is assigned to O^{2-} ions at a binding energy of 531.2 eV in the Zn–O bonding of the hexagonal structure of ZnO. The convoluted peak at 532.9 eV is attributed to O^{-} and O^{2-} ions in oxygen-deficient regions in the HFNZO surface[42], [43].In the Ni 2p core-level spectrum ~861.2 and 883eV show that these

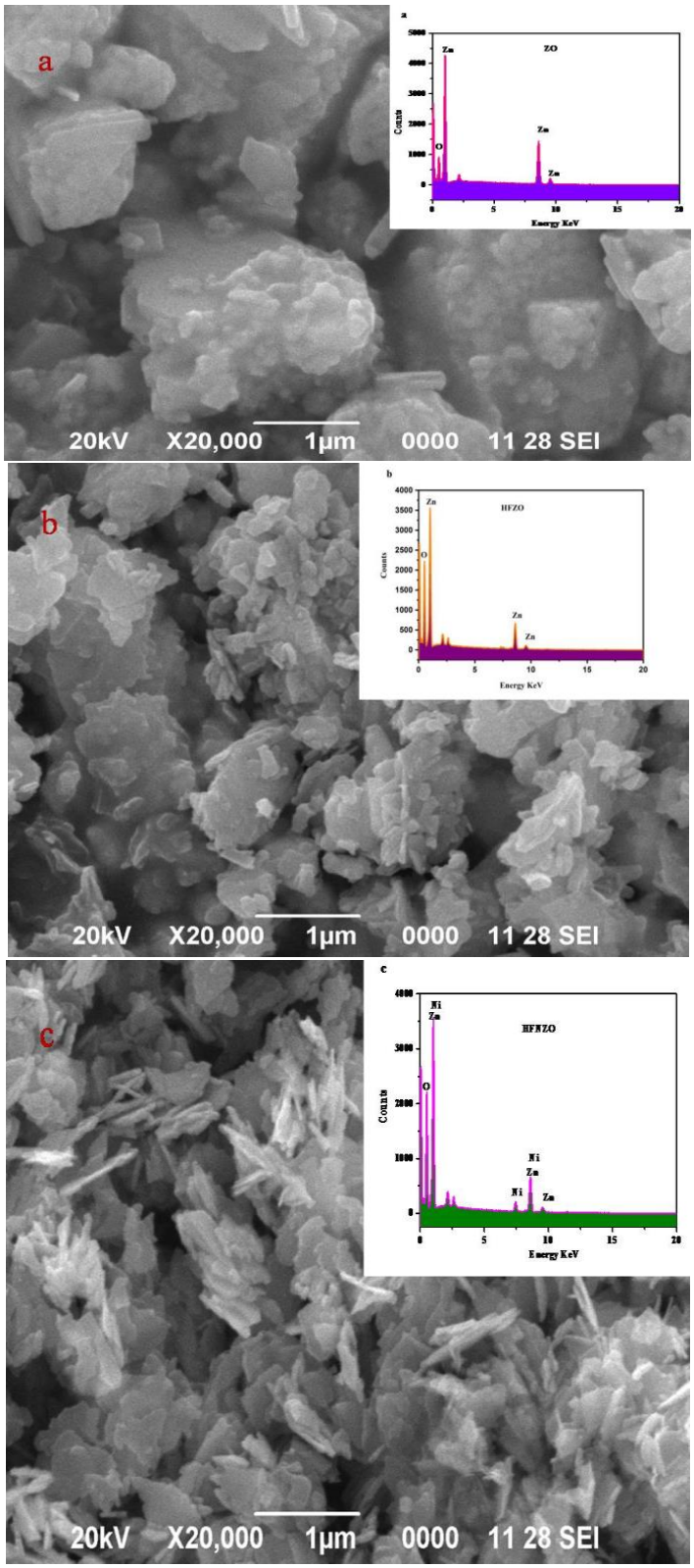

Fig. 6. (a) Morphological structure image and EDX of ZO (b) Morphological structure image and EDX of HFZO (c) Morphological structure image and EDX of HFNZO

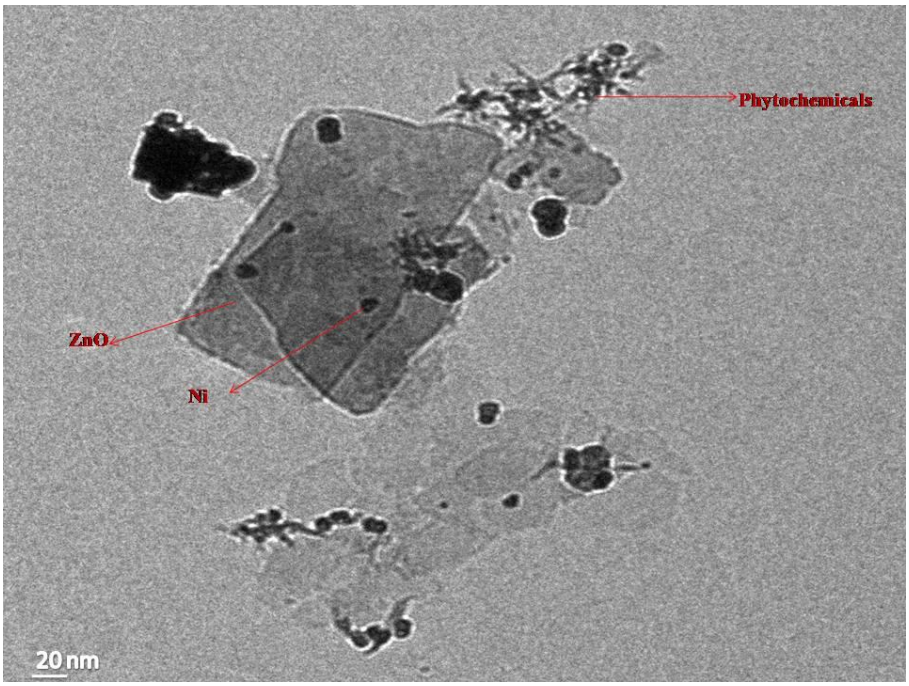

Fig. 7 TEM image of HFNZO

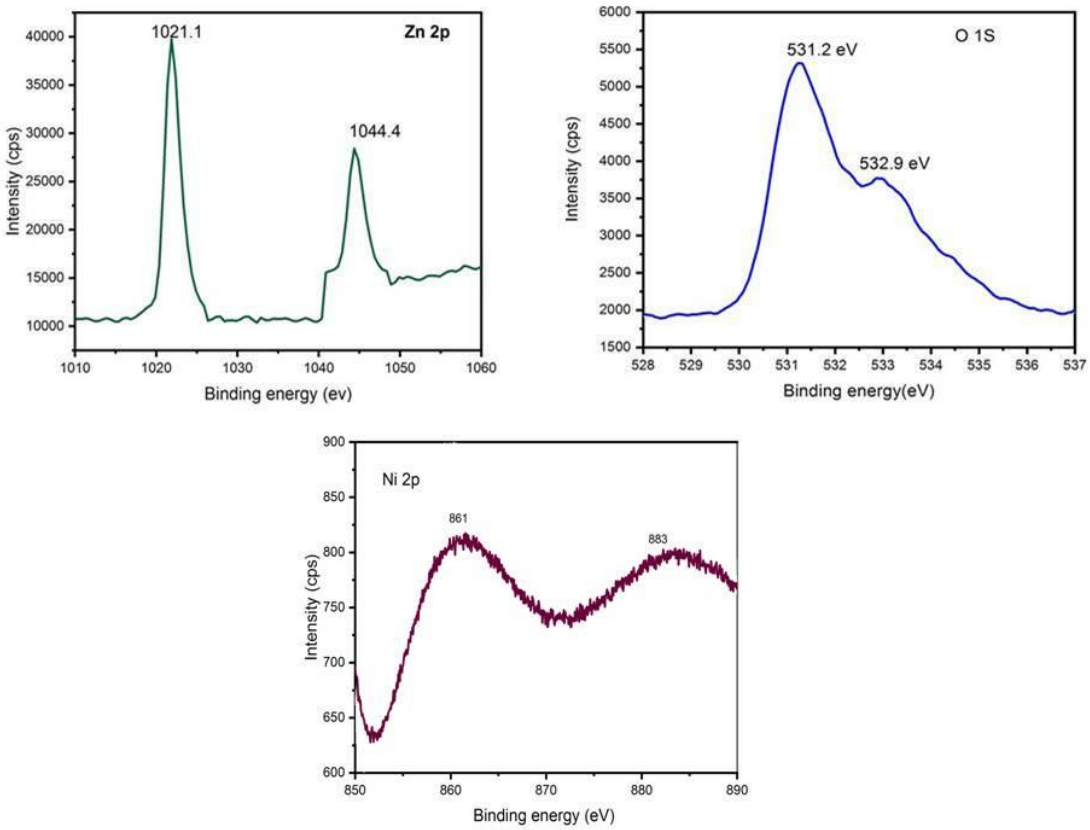

Fig. 8 High-resolution XPS of Zn 2p, Ni 2p, and O 1s XPS spectra.

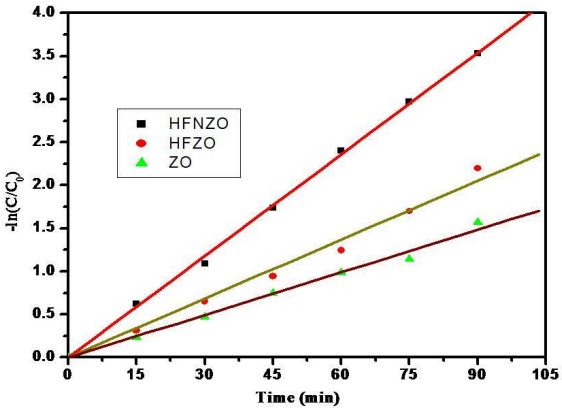

Fig. 9. Photodegradation of RA and Its kinetic plot

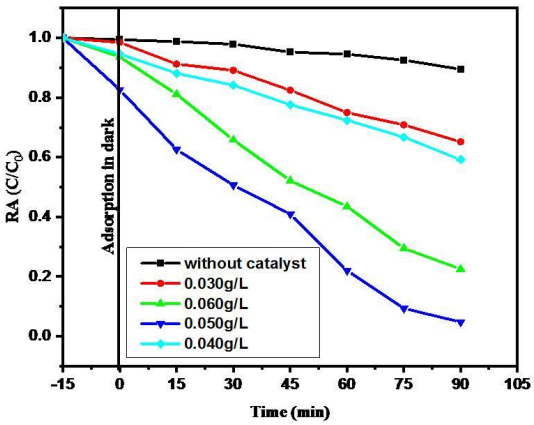

Fig. 10. Photodegradation of RA using HFNZO

peaks are attributed to Ni in the form of oxide and hydroxide phases.

Visible Light Photocatalytic Evaluation

The photocatalytic activity of HFNZO was measured in an aqueous solution of RA at 20 μM at a catalyst concentration of 0.050 g/L, and after irradiation for 90 min. In Fig. 6, the absorption spectra of RA under visible light irradiation with HFNZO are shown. As the irradiation period increases, the strength of the absorption peak at λ=540 nm steadily declines until it practically vanishes at 90 min, showing the degradation of RA by the photocatalytic activity of HFNZO. In the absence of a photocatalyst, the least amount of RA degradation results from chemical reactions rather than adsorption. A pseudo-first-order kinetic model was developed to compare the reaction rates of various nanoparticles in equation (4),

$$-ln\frac{C}{C_0} = kt \qquad (4)$$

where C_0 was the original RA concentration at time t=0 min, C was the initial MB concentration at time t of illumination, and k was the rate constant. In Fig. 9, a linear relationship between the variables -ln (C/C_0) and irradiation time 't' was shown. We assume that the amount of RA following desorption-adsorption equilibrium is the starting concentration C_0 given the experimental setup[34], [44]. The rate constants k of HFNZO, HFZO, and ZO are determined to be 3.93×10^{-2} s^{-1}, 2.279×10^{-2} s^{-1}, and 1.648×10^{-3} s^{-1}, respectively, based on the kinetic model mentioned above. Therefore, surface modification with plant extract and dopants, especially Ni^{2+}, dramatically increases ZnO reactivity toward visible light.

The photocatalytic activity of the HFNZO sample is greater than that of pure ZO. New impurity levels between the conduction and valence bands are generated in the lattice of ZnO when Ni^{2+} is substituted, and electrons can be promoted from the valence band to these impurity levels[49]. The photocatalytic activities may then attract more photogenerated electrons and holes as a result. Since the band gap of the HFNZO sample is less than that of pure ZnO, it may increase the absorption of visible light. In addition to this result, Ni^{2+} ions can act as charge carrier (e^- or h^+) shallow trapping sites in photocatalytic reactions, as reported in [50]:

$$Phytochemicals + h\gamma \rightarrow Phytochemcials^* + e^- \qquad 1$$

$$Ni^{2+} + e^- \rightarrow Ni^+ \qquad 2$$

$$Ni^+ + O_2 \rightarrow Ni^{2+} + O_2^- \qquad 3$$

$$Ni^{2+} + h^+ \rightarrow Ni^{3+} \qquad 4$$

$$Ni^{3+} + OH \rightarrow Ni^{2+} + OH^- \qquad 5$$

Ni^{2+} serves as an electron and hole trap and its ability to separate the arrival time to the solution phase (Eqs. (3) and (5)) or the substrate result in a reduction in the electron-hole pair combining rate and an increase in photocatalytic activity.

Choosing the appropriate catalyst loading for optimal degradation is desirable to avoid the usage of excess catalysts. A series of tests were performed with a catalyst dosage ranging from 0.030 to 0.060 g/L, a dye concentration of 20 μM, and a 90-minute irradiation period. Fig. 10 shows the degradation

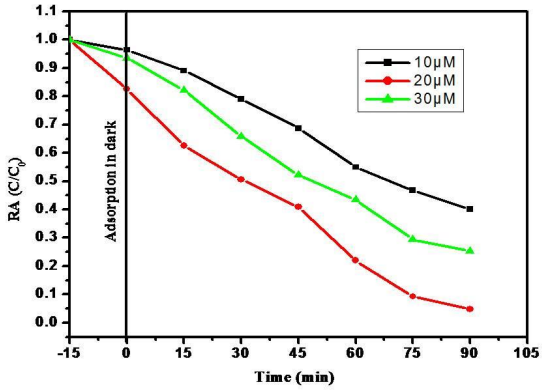

Fig.11. Initial concentration of RA dye

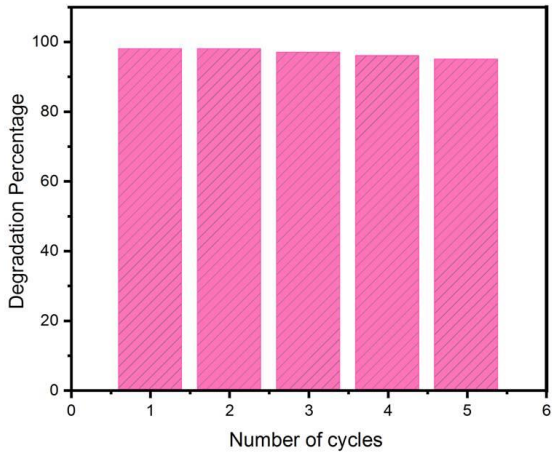

Fig.12 The efficiency of reuse of HFNZO

Table 1. The comparison of photodegradation (%) was reported by various researchers using various dyes.

Photocatalysis	Model pollutant	Percentage of degradation	Reference
PSf/Ni@ZnO	Methylene Blue	80	[45]
N-CQDs/Ni-ZnO	Methylene Blue	86	[46]
Co-doped ZnO	Methylene Blue	86	[47]
Ni/ZnO	Methylene Blue	92	[48]
HFNZO	Rose Aniline	98 (90 min)	In this study

efficiency of RA for different photocatalyst loadings. The results indicate that the dye degradation dramatically increases from about 59% to nearly 95% with an increase in catalyst loading from 0.030 to 0.050 g/L. This is because increasing the catalyst loading increases the active sites on the surface of the catalyst, which in turn increases the amount of RA species that can bind to the surface [51]. As an outcome, greater catalyst loading increases degrading efficiency. The degradation rate reduces as catalyst loading is raised from 0.050 to 0.060 g/L, indicating an increase in total active surface area and the availability of additional active sites for photoreaction. As a result, the suspension's turbidity increased, which has the effect of blocking out visible light. For this concentration of RA (20 mg/L), the catalyst efficiency has been brought to an optimal point. A further increase in catalyst dosage over 0.050 g/L caused a decrease in dye degradation. This condition might be brought on by an excess of photocatalyst particles that prevents and blocks light from passing through. On the other hand, particle aggregation is significant at high catalyst concentrations, which reduces the active sites on the catalyst surface.

The impact of initial dye concentration on the degradation of RA is shown in Fig. 11. Initial RA dye concentrations ranged from 10 to 30 μM. With an increase in MB (10–20 μM), the photodegradation of RA rises and then falls with an increase in concentration (20–30 μM). The concentration has a negative effect on the photodegradation efficiency. The equilibrium adsorption of dye on the catalyst surface, which leads to a reduction in the number of active sites, was thought to explain why degradation decreased as dye concentration increased. Hydroxyl radicals, which are thought to be the dye's major oxidizing agent, are produced as a result of this occurrence[52][53]. The initial concentration is inversely correlated with the number of organic compounds that are adsorbed on the catalyst surface and the degree of coloration of the solution. As a result, there will be fewer active sites for OH- adsorption, which will lower the amount of OH- generated[54]. A further increase in RA concentration may result in a reduced photon penetration path into the aqueous solution of RA and a decrease in the catalytic activity.

The reusability and stability of a photocatalyst are very important things for its practical application. The catalyst is recovered after each cycle by centrifugation, dried in a hot air oven for 4 hours then reused. The results of the recycle photocatalyst for HFNZO are depicted in Fig. 12. As shown in the figure, HFNZO showed 98%photocatalytic activity in the first two cycles and from Table 1 literature review photocatalyst. After the third reuse, there is a decrease in the degradation due to the loss of catalyst during washing. The recycling experiments imply that HFNZO might be effectively used for the degradation of organic pollutants in water[52].

CONCLUSION

In this study, HFNZO nanoparticles were successfully synthesized to remove methylene blue dye from an aqueous solution using Fresh Hibiscus rosasinensis flower extract as a surface modifier. The photocatalyst of HFNZO is successful for dye RA when subjected to visible light irradiation. Most importantly, the system could show a 98% photodegradation efficiency for the model pollutants, due to slow electron-hole recombination rate. The results showed that these HFNZO nanoparticles possessed well crystallinity and significant optical properties. These nanoparticles have good nanostructures and resulting in a remarkable photocatalytic performance in the photocatalytic degradation of RA dye under visible light within 90 min at a dye concentration of 20 μM with a nanoparticles dosage of 0.050 g/L. The results also indicate the possibility that employing the photocatalyst in its current state will aid in the degradation of organic dyes that have better stability, conformity, and optical characteristics, which will help to address environmental issues.

CONFLICT OF INTEREST

The authors hereby declare that there is no conflict of interest.

REFERENCE

[1] C. Galindo, P. Jacques, and A. Kalt, "Photochemical and photocatalytic degradation of an indigoid dye: a case study of acid blue 74 (AB74)," J PhotochemPhotobiolA Chem, vol. 141, no. 1, pp. 47-56, Jun. 2001, doi: 10.1016/S1010-6030(01)00435-X. https://doi.org/10.1016/S1010-6030(01)00435-X

[2] W. M. Li et al., "Superconductivity in a unique type of copper oxide," Proceedings of the National Academy of Sciences, vol. 116, no. 25, pp. 12156-12160, Jun. 2019, doi: 10.1073/pnas.1900908116. https://doi.org/10.1073/pnas.1900908116

[3] W. Muzafaret al., "Green synthesis of iron oxide nanoparticles using Melia azedarach flowers extract and evaluation of their antimicrobial and antioxidant activities," J Mol Struct, vol. 1269, p. 133824, Dec. 2022, doi: 10.1016/J.MOLSTRUC.2022.133824. https://doi.org/10.1016/j.molstruc.2022.133824

[4] A. Criscuoli, "Vacuum Membrane Distillation (VMD), Applications of," in Encyclopedia of Membranes, Berlin, Heidelberg: Springer Berlin Heidelberg, 2014, pp. 1-2. doi: 10.1007/978-3-642-40872-4_777-2. https://doi.org/10.1007/978-3-642-40872-4_777-2

[5] N. Daneshvar, M. Rabbani, N. Modirshahla, and M. A. Behnajady, "Kinetic modeling of photocatalytic degradation of Acid Red 27 in UV/TiO2 process," J PhotochemPhotobiolA Chem, vol. 168, no. 1-2, pp. 39-45, Nov. 2004, doi: 10.1016/j.jphotochem.2004.05.011. https://doi.org/10.1016/j.jphotochem.2004.05.011

[6] J. Sun, Y. Wang, R. Sun, and S. Dong, "Photodegradation of azo dye Congo Red from aqueous solution by the WO3-TiO2/activated carbon (AC) photocatalyst under the UV irradiation," Mater Chem Phys, vol. 115, no. 1, pp. 303-308, May 2009, doi: 10.1016/j.matchemphys.2008.12.008. https://doi.org/10.1016/j.matchemphys.2008.12.008

[7] A. Nageswara Rao, B. Sivasankar, and V. Sadasivam, "Kinetic study on the photocatalytic degradation of salicylic acid using ZnO catalyst," J Hazard Mater, vol. 166, no. 2-3, pp. 1357-1361, Jul. 2009, doi: 10.1016/J.JHAZMAT.2008.12.051. https://doi.org/10.1016/j.jhazmat.2008.12.051

[8] J. Wang et al., "Sonocatalytic degradation of some dyestuffs and comparison of catalytic activities of nano-sized TiO2, nano-sized ZnO and composite TiO2/ZnO powders under ultrasonic irradiation," UltrasonSonochem, vol. 16, no. 2, pp. 225-231, Feb. 2009, doi: 10.1016/J.ULTSONCH.2008.08.005. https://doi.org/10.1016/j.ultsonch.2008.08.005

[9] Y. Yan et al., "Microwave-assisted in situ synthesis of reduced graphene oxide-BiVO4 composite photocatalysts and their enhanced photocatalytic performance for the degradation of ciprofloxacin," J Hazard Mater, vol. 250-251, pp. 106-114, Apr. 2013, doi: 10.1016/J.JHAZMAT.2013.01.051. https://doi.org/10.1016/j.jhazmat.2013.01.051

[10] J. C. Lee, S. Park, H.-J. Park, J.-H. Lee, H.-S. Kim, and Y.-J. Chung, "Photocatalytic degradation of TOC from aqueous phenol solution using solution combusted ZnO nanopowders," J Electroceram, vol. 22, no. 1-3, pp. 110-113, Feb. 2009, doi: 10.1007/s10832-007-9356-3. https://doi.org/10.1007/s10832-007-9356-3

[11] A. A. Khassinet al., "Metal-support interactions in cobalt-aluminum co-precipitated catalysts: XPS and CO adsorption studies," J Mol CatalA Chem, vol. 175, no. 1-2, pp. 189-204, Oct. 2001, doi: 10.1016/S1381-1169(01)00216-3. https://doi.org/10.1016/S1381-1169(01)00216-3

[12] E. Chamanehpour, M. H. Sayadi, and M. Hajiani, "A hierarchical graphitic carbon nitride supported by metal-organic framework and copper nanocomposite as a novel bifunctional catalyst with long-term stability for enhanced carbon dioxide photoreduction under solar light irradiation," Adv Compos Hybrid Mater, vol. 5, no. 3, pp. 2461-2477, Sep. 2022, doi: 10.1007/s42114-022-00459-6. https://doi.org/10.1007/s42114-022-00459-6

[13] J. N. Hasnidawani, H. N. Azlina, H. Norita, N. N. Bonnia, S. Ratim, and E. S. Ali, "Synthesis of ZnO Nanostructures Using Sol-Gel Method," Procedia Chem, vol. 19, pp. 211-216, Jan. 2016, doi: 10.1016/J.PROCHE.2016.03.095.

https://doi.org/10.1016/j.proche.2016.03.095
[14] N. Sharma and P. P. Sahay, "Solution combustion synthesis of Dy-doped ZnO nanoparticles: An investigation of their structural, optical and photoluminescence characteristics," J Lumin, vol. 257, p. 119655, May 2023, doi: 10.1016/J.JLUMIN.2022.119655. https://doi.org/10.1016/j.jlumin.2022.119655
[15] A. S. Parlakyigit, C. Ergun, and O. Gokcekaya, "Synthesis of ZnO nanoparticles via spray atomization assisted inductively coupled plasma technique," Ceram Int, Apr. 2023, doi: 10.1016/J.CERAMINT.2023.04.129. https://doi.org/10.1016/j.ceramint.2023.04.129
[16] R. Kumar Pandey, H. Choi, J. Yi, J. Heo, and P. Kumar Sahu, "Facile controlled synthesis of bifunctional ZnO nanoparticles for application as a high-performance self-powered UV photosensor and highly selective vapor sensor," Materials Science and Engineering: B, vol. 293, p. 116470, Jul. 2023, doi: 10.1016/J.MSEB.2023.116470. https://doi.org/10.1016/j.mseb.2023.116470
[17] R. Ullah and M. Tuzen, "Facile hydrothermal synthesis of ZnO nanoparticles on silicalite-1: Effect of ultra ZnO Nano size on desulfurization activities," Surfaces and Interfaces, vol. 39, p. 102918, Jul. 2023, doi: 10.1016/J.SURFIN.2023.102918. https://doi.org/10.1016/j.surfin.2023.102918
[18] S. Prabhu, T. Daniel Thangadurai, T. Indumathi, and P. Kalugasalam, "Enhanced visible light induced dye degradation and antibacterial activities of ZnO/NiO nanocomposite synthesized using Clitoriaternatea flower extract," Inorg Chem Commun, vol. 146, p. 110077, Dec. 2022, doi: 10.1016/J.INOCHE.2022.110077. https://doi.org/10.1016/j.inoche.2022.110077
[19] N. T. T. Nguyen et al., "Green synthesis of ZnFe2O4@ZnO nanocomposites using Chrysanthemum spp. floral waste for photocatalytic dye degradation," J Environ Manage, vol. 326, p. 116746, Jan. 2023, doi: 10.1016/J.JENVMAN.2022.116746. https://doi.org/10.1016/j.jenvman.2022.116746
[20] A. K. Prajapati and M. K. Mondal, "Novel green strategy for CuO-ZnO-C nanocomposites fabrication using marigold (Tagetes spp.) flower petals extract with and without CTAB treatment for adsorption of Cr(VI) and Congo red dye," J Environ Manage, vol. 290, p. 112615, Jul. 2021, doi: 10.1016/J.JENVMAN.2021.112615. https://doi.org/10.1016/j.jenvman.2021.112615
[21] S. Zeghoudet al., "A review on biogenic green synthesis of ZnO nanoparticles by plant biomass and their applications," Mater Today Commun, vol. 33, p. 104747, Dec. 2022, doi: 10.1016/J.MTCOMM.2022.104747. https://doi.org/10.1016/j.mtcomm.2022.104747
[22] F. P. Araujo et al., "Eco-friendly synthesis and photocatalytic application of flowers-like ZnO structures using Arabic and Karaya Gums," Int J Biol Macromol, vol. 165, pp. 2813-2822, Dec. 2020, doi: 10.1016/J.IJBIOMAC.2020.10.132. https://doi.org/10.1016/j.ijbiomac.2020.10.132
[23] D. Garg, A. Shaikh, A. Muley, and T. Marar, "In-vitro antioxidant activity and phytochemical analysis in extracts of Hibiscus rosa-sinensis stem and leaves," Free Radicals and Antioxidants, vol. 2, no. 3, pp. 41-46, Jul. 2012, doi: 10.5530/AX.2012.3.6. https://doi.org/10.5530/ax.2012.3.6
[24] G. Riaz and R. Chopra, "A review on phytochemistry and therapeutic uses of Hibiscus sabdariffa L.," Biomedicine & Pharmacotherapy, vol. 102, pp. 575-586, Jun. 2018, doi: 10.1016/j.biopha.2018.03.023. https://doi.org/10.1016/j.biopha.2018.03.023
[25] Y. W. Mak, L. O. Chuah, R. Ahmad, and R. Bhat, "Antioxidant and antibacterial activities of hibiscus (Hibiscus rosa-sinensis L.) and Cassia (Senna bicapsularis L.) flower extracts," J King Saud Univ Sci, vol. 25, no. 4, pp. 275-282, Oct. 2013, doi: 10.1016/J.JKSUS.2012.12.003. https://doi.org/10.1016/j.jksus.2012.12.003
[26] H. Benelmadjat, B. Boudine, O. Halimi, and M. Sebais, "Fabrication and characterization of pure and Sn/Sb-doped ZnO thin films deposited by sol-gel method," Opt Laser Technol, vol. 41, no. 5, pp. 630-633, Jul. 2009, doi: 10.1016/J.OPTLASTEC.2008.09.011. https://doi.org/10.1016/j.optlastec.2008.09.011
[27] A. A. Aboud, M. Shaban, and N. Revaprasadu, "Effect of Cu, Ni and Pb doping on the photo-electrochemical activity of ZnO thin films," RSC Adv, vol. 9, no. 14, pp. 7729-7736, 2019, doi: 10.1039/C8RA10599E. https://doi.org/10.1039/C8RA10599E
[28] K. Vignesh, R. Hariharan, M. Rajarajan, and A. Suganthi, "Photocatalytic performance of Ag doped SnO2 nanoparticles modified with curcumin," Solid State Sci, vol. 21, pp. 91-99, Jul. 2013, doi: 10.1016/J.SOLIDSTATESCIENCES.2013.04.017. https://doi.org/10.1016/j.solidstatesciences.2013.04.017
[29] P. Pascariu, I. V. Tudose, M. Suchea, E. Koudoumas, N. Fifere, and A. Airinei, "Preparation and characterization of Ni, Co doped ZnO nanoparticles for photocatalytic applications," Appl Surf Sci, vol. 448, pp. 481-488, Aug. 2018, doi: 10.1016/J.APSUSC.2018.04.124. https://doi.org/10.1016/j.apsusc.2018.04.124
[30] R. Karthiga, B. Kavitha, M. Rajarajan, and A. Suganthi, "Synthesis of MoO3 microrods via phytoconsituents of Azadirachtaindica leaf to study the cationic dye degradation and antimicrobial properties," J Alloys Compd, vol. 753, pp. 300-307, Jul. 2018, doi: 10.1016/j.jallcom.2018.04.230. https://doi.org/10.1016/j.jallcom.2018.04.230
[31] L. Yang, L. E. Yu, and M. B. Ray, "Degradation of paracetamol in aqueous solutions by TiO2 photocatalysis," Water Res, vol. 42, no. 13, pp. 3480-3488, Jul. 2008, doi: 10.1016/j.watres.2008.04.023. https://doi.org/10.1016/j.watres.2008.04.023
[32] A. Rezaei, M. R. Rezaei, and M. H. Sayadi, "3D network structure graphene hydrogel-Fe3O4@SnO2/Ag via an adsorption/photocatalysis synergy for removal of 2,4 dichlorophenol," J Taiwan Inst Chem Eng, vol. 121, pp. 154-167, Apr. 2021, doi: 10.1016/j.jtice.2021.03.048. https://doi.org/10.1016/j.jtice.2021.03.048
[33] S. Faisal et al., "Green Synthesis of Zinc Oxide (ZnO) Nanoparticles Using Aqueous Fruit Extracts of Myristicafragrans : Their Characterizations and Biological and Environmental Applications," ACS Omega, vol. 6, no. 14, pp. 9709-9722, Apr. 2021, doi: 10.1021/acsomega.1c00310. https://doi.org/10.1021/acsomega.1c00310
[34] N. Ahmadpour, M. H. Sayadi, and S. Homaeigohar, "A hierarchical Ca/TiO2/NH2-MIL-125 nanocomposite photocatalyst for solar visible light induced photodegradation of organic dye pollutants in water," RSC Adv, vol. 10, no. 50, pp. 29808-29820, Aug. 2020, doi: 10.1039/d0ra05192f. https://doi.org/10.1039/D0RA05192F
[35] R. Karthiga, B. Kavitha, M. Rajarajan, and A. Suganthi, "Photocatalytic and antimicrobial activity of NiWO4 nanoparticles stabilized by the plant extract," Mater Sci Semicond Process, vol. 40, pp.

123-129, Dec. 2015, doi: 10.1016/j.mssp.2015.05.037. https://doi.org/10.1016/j.mssp.2015.05.037

[36] K. Rajendaran, R. Muthuramalingam, and S. Ayyadurai, "Green synthesis of Ag-Mo/CuO nanoparticles using Azadirachtaindica leaf extracts to study its solar photocatalytic and antimicrobial activities," Mater Sci Semicond Process, vol. 91, pp. 230-238, Mar. 2019, doi: 10.1016/j.mssp.2018.11.021. https://doi.org/10.1016/j.mssp.2018.11.021

[37] A. P. Vijayaparkavi and S. Senthilkumaar, "Synthesis and Characterization of ZnO and Ni Doped ZnO," J Supercond Nov Magn, vol. 25, no. 2, pp. 427-433, Feb. 2012, doi: 10.1007/s10948-011-1278-2. https://doi.org/10.1007/s10948-011-1278-2

[38] M. N. Siddique, T. Ali, A. Ahmed, and P. Tripathi, "Enhanced electrical and thermal properties of pure and Ni substituted ZnO Nanoparticles," Nano-Structures & Nano-Objects, vol. 16, pp. 156-166, Oct. 2018, doi: 10.1016/j.nanoso.2018.06.001. https://doi.org/10.1016/j.nanoso.2018.06.001

[39] H. Singh, V. Kumar, H. C. Jeon, T. W. Kang, and S. Kumar, "Structural, optical and electrical properties of Ni doped ZnO nanostructures synthesized by solution combustion method," Journal of Materials Science: Materials in Electronics, vol. 29, no. 2, pp. 1327-1332, Jan. 2018, doi: 10.1007/s10854-017-8038-4. https://doi.org/10.1007/s10854-017-8038-4

[40] K. Arora, "POLLEN IDENTIFICATION OF HIBISCUS ROSA-SINENSIS AND SIDA ACUTA THROUGH FTIR SPECTROSCOPY," 2014. [Online]. Available: http://www.cibtech.org/jls.htm

[41] K. L. Foo, U. Hashim, K. Muhammad, and C. H. Voon, "Sol-gel synthesized zinc oxide nanorods and their structural and optical investigation for optoelectronic application," Nanoscale Res Lett, vol. 9, no. 1, p. 429, Dec. 2014, doi: 10.1186/1556-276X-9-429. https://doi.org/10.1186/1556-276X-9-429

[42] W. Liu, X. Tang, Z. Tang, F. Chu, T. Zeng, and N. Tang, "Role of oxygen defects in magnetic property of Cu doped ZnO," J Alloys Compd, vol. 615, pp. 740-744, Dec. 2014, doi: 10.1016/j.jallcom.2014.07.033. https://doi.org/10.1016/j.jallcom.2014.07.033

[43] S. A. Al-Ghamdiet al., "Photocatalytic degradation of potassium permanganate using zinc oxide nanoparticles," Dig J NanomaterBiostruct, vol. 16, no. 3, pp. 889-898, Jul. 2021, doi: 10.15251/DJNB.2021.163.889. https://doi.org/10.15251/DJNB.2021.163.889

[44] F. Kargar, A. Bemani, M. H. Sayadi, and N. Ahmadpour, "Synthesis of modified beta bismuth oxide by titanium oxide and highly efficient solar photocatalytic properties on hydroxychloroquine degradation and pathways," J PhotochemPhotobiolA Chem, vol. 419, Oct. 2021, doi: 10.1016/j.jphotochem.2021.113453. https://doi.org/10.1016/j.jphotochem.2021.113453

[45] L. H. Mohammed, F. Gulbagca, R. N. E. Tiri, A. Aygun, M. Bekmezci, and F. Sen, "Hydrothermal-assisted synthesis of Co-doped ZnO nanoparticles catalyst for sodium borohydride dehydrogenation and photodegradation of organic pollutants in water," Chemical Engineering Journal Advances, vol. 14, p. 100495, May 2023, doi: 10.1016/J.CEJA.2023.100495. https://doi.org/10.1016/j.ceja.2023.100495

[46] R. Behnood and G. Sodeifian, "Synthesis of N doped-CQDs/Ni doped-ZnO nanocomposites for visible light photodegradation of organic pollutants," J Environ Chem Eng, vol. 8, no. 4, p. 103821, Aug. 2020, doi: 10.1016/J.JECE.2020.103821. https://doi.org/10.1016/j.jece.2020.103821

[47] P. Pascariu, I. V. Tudose, M. Suchea, E. Koudoumas, N. Fifere, and A. Airinei, "Preparation and characterization of Ni, Co doped ZnO nanoparticles for photocatalytic applications," Appl Surf Sci, vol. 448, pp. 481-488, Aug. 2018, doi: 10.1016/J.APSUSC.2018.04.124. https://doi.org/10.1016/j.apsusc.2018.04.124

[48] B. Bhushan, K. Jahan, V. Verma, B. S. Murty, and K. Mondal, "Photodegradation of methylene blue dye by powders of Ni-ZnO floweret consisting of petals of ZnO nanorod around Ni-rich core," Mater Chem Phys, vol. 253, p. 123394, Oct. 2020, doi: 10.1016/J.MATCHEMPHYS.2020.123394. https://doi.org/10.1016/j.matchemphys.2020.123394

[49] M. H. Sayadi, S. Ghollasimood, N. Ahmadpour, and S. Homaeigohar, "Biosynthesis of the ZnO/SnO2 nanoparticles and characterization of their photocatalytic potential for removal of organic water pollutants," J PhotochemPhotobiolA Chem, vol. 425, p. 113662, Mar. 2022, doi: 10.1016/J.JPHOTOCHEM.2021.113662. https://doi.org/10.1016/j.jphotochem.2021.113662

[50] M. Khalatbary, M. H. Sayadi, M. Hajiani, M. Nowrouzi, and S. Homaeigohar, "Green, Sustainable Synthesis of γ-Fe2O3/MWCNT/Ag Nano-Composites Using the Viscum album LeafExtractandWasteCarTireforRemovalofSulfamethazine and Bacteria from Wastewater Streams," Nanomaterials, vol. 12, no. 16, Aug. 2022, doi: 10.3390/nano12162798. https://doi.org/10.3390/nano12162798

[51] E. Chamanehpour, M. Hossein Sayadi, and M. Hajiani, "Metal-organic framework coordinated with g-C3N4 and metal ions for boosting photocatalytic H2 production under sunlight," J PhotochemPhotobiolA Chem, vol. 434, Jan. 2023, doi: 10.1016/j.jphotochem.2022.114221. https://doi.org/10.1016/j.jphotochem.2022.114221

[52] F. Poorsajadi, M. H. Sayadi, M. Hajiani, and M. R. Rezaei, "Synthesis of CuO/Bi2O3 nanocomposite for efficient and recycling photodegradation of methylene blue dye," Int J Environ Anal Chem, vol. 102, no. 18, pp. 7165-7178, 2022, doi: 10.1080/03067319.2020.1826464. https://doi.org/10.1080/03067319.2020.1826464

[53] M. H. Sayadi, N. Ahmadpour, and S. Homaeigohar, "Photocatalytic and antibacterial properties of Ag-CuFe2O4 @WO3 magnetic nanocomposite," Nanomaterials, vol. 11, no. 2, pp. 1-19, Feb. 2021, doi: 10.3390/nano11020298. https://doi.org/10.3390/nano11020298

[54] S. Mohammadi-Aghdam, R. Marandi, M. E. Olya, and A. A. Mehrdad Sharif, "Kinetic modeling of BB41 photocatalytic treatment in a semibatch flow photoreactor using a nano composite film," Journal of Saudi Chemical Society, vol. 18, no. 4, pp. 317-326, 2014, doi: 10.1016/j.jscs.2013.09.012. https://doi.org/10.1016/j.jscs.2013.09.012